Characteristics of phonation onset in a two-layer vocal fold model

Zhaoyan Zhang[a)]
School of Medicine, University of California, Los Angeles, 31-24 Rehabilitation Center, 1000 Veteran Avenue, Los Angeles, California 90095-1794

(Received 10 June 2008; revised 14 October 2008; accepted 21 November 2008)

Characteristics of phonation onset were investigated in a two-layer body-cover continuum model of the vocal folds as a function of the biomechanical and geometric properties of the vocal folds. The analysis showed that an increase in either the body or cover stiffness generally increased the phonation threshold pressure and phonation onset frequency, although the effectiveness of varying body or cover stiffness as a pitch control mechanism varied depending on the body-cover stiffness ratio. Increasing body-cover stiffness ratio reduced the vibration amplitude of the body layer, and the vocal fold motion was gradually restricted to the medial surface, resulting in more effective flow modulation and higher sound production efficiency. The fluid-structure interaction induced synchronization of more than one group of eigenmodes so that two or more eigenmodes may be simultaneously destabilized toward phonation onset. At certain conditions, a slight change in vocal fold stiffness or geometry may cause phonation onset to occur as eigenmode synchronization due to a different pair of eigenmodes, leading to sudden changes in phonation onset frequency, vocal fold vibration pattern, and sound production efficiency. Although observed in a linear stability analysis, a similar mechanism may also play a role in register changes at finite-amplitude oscillations.
 [DOI: 10.1121/1.3050285]

PACS number(s): 43.70.Bk, 43.70.Gr [AL] Pages: 1091–1102

I. INTRODUCTION

The vocal folds are complex layered structures consisting of a muscular layer at the base, multiple layers of lamina propria in the middle, and an outmost epithelium layer. The geometry and mechanical properties of these different layers can be altered by laryngeal adjustments or due to vocal pathologies. Such changes often lead to qualitatively distinct vocal fold vibration and voice quality (Titze, 1994; Colton and Casper, 1996). An ultimate goal of voice production research is to understand and predict the acoustic consequences of such changes in geometry and biomechanical properties of the vocal folds. The influence on phonation onset frequency, phonation threshold pressure, and vocal fold vibration characteristics is of particular interest.

The influence of biomechanical properties of the vocal folds on phonation has been the focus of many previous works. Due to their simplicity, lumped-mass models were often used in these studies. For example, based on a body-cover representation of the vocal fold, Titze *et al.* (1988) used a string model to study pitch control mechanisms in human phonation. They showed that although the contraction of the cricothyroid (CT) muscle always causes the phonation frequency to increase, the contraction of the thyroarytenoid (TA) muscle may decrease or increase the phonation frequency depending on the effective depth of the vocal fold in vibration. Using a three-mass body-cover model, Story and Titze (1995) showed that a variety of vocal fold vibration patterns can be produced using different combinations of body and cover stiffnesses. Increasing body stiffness generally leads to lower body layer amplitudes and higher pitches. In a recent study, Tokuda *et al.* (2007) used a three-mass cover-only model to study chest-falsetto register transition (a sudden qualitative change in vocal fold vibration pattern, see, e.g., Titze, 1994; Svec *et al.*, 1999). They showed that such an abrupt transition occurs as a spontaneous shift in dominance between different eigenmodes of the vocal folds. In their study, such shift was induced by variation in the stiffness of the middle mass, which caused the vocal fold vibration to switch from being dominated by the first eigenmode of the vocal folds to being dominated by the third eigenmode of the vocal folds.

Although lumped-mass models provide valuable insights into the physics of phonation, their use in practical applications is limited. Because of the lack of direct correspondence to realistic, directly measurable properties of the vocal folds, model parameters of lumped-mass models need to be estimated. This is often difficult, if not impossible, as some model parameters are dynamic variables of the coupled fluid-structure system, which cannot be determined *a priori*. For example, Titze *et al.* (1988) showed that the effective depth of vibration is an important factor in the determination of phonation frequency. However, evaluation of the effective depth of vibration requires information on the vibration field within the vocal fold structure, which is generally unknown and highly depends on the specific biomechanical properties of the vocal folds. It is still unknown how much control the human has over the effective depth of vibration (Titze *et al.*, 1988). Similarly, the coupling stiffness between the upper and lower masses in the two-mass model and its variants (e.g., Ishizaka and Flanagan, 1972; Story and Titze, 1995) determines the phase difference between the two masses and

[a)]Electronic mail: zyzhang@ucla.edu

therefore the phonation threshold pressure (Titze, 1988). However, it remains unknown how the body and cover stiffnesses would affect this coupling stiffness. Estimation of these important model parameters is extremely difficult and often requires knowledge of the vocal fold vibration field that is to be solved for. This difficulty makes the lumped-mass models less appealing for use in practical applications in which the influence of the realistic vocal fold geometry and changes in local biomechanical properties needs to be evaluated. Furthermore, lumped-mass models may have oversimplified the underlying physics of phonation. For example, the superior-inferior component of the vocal fold motion, which has been shown to have a pronounced effect on phonation (Ishizaka and Flanagan, 1977; Titze and Talkin, 1979; Zhang *et al.*, 2006a, 2006b), was often neglected in lumped-mass models of phonation.

For practical applications, a better description of the underlying physics and a realistic representation of the vocal fold geometry are required. Based on continuum mechanics, continuum models allow vocal fold dynamics to be calculated from directly measurable parameters such as biomechanical properties (or preferably the degree of laryngeal muscle contraction) and realistic geometric parameters of the vocal folds. Recent studies (Zhang *et al.*, 2006a; Zhang, 2008) show that geometric details of the vocal folds may have a large impact on vocal fold vibration. A better understanding of how realistic vocal fold geometry would affect the vocal fold eigenmodes and the eigenmode synchronization process may also provide new insights into mechanisms of register change. Furthermore, continuum models allow a natural representation of the biomechanics of the layered structure of the vocal folds. Such realistic representation of the vocal fold biomechanics is particularly critical for the modeling of vocal pathologies, for which changes in biomechanical properties are often localized (e.g., local stiffening due to vocal fold scarring).

There has been an increasing amount of work on continuum modeling of phonation (e.g., Titze and Talkin, 1979; Alipour *et al.*, 2000; De Oliveira Rosa *et al.*, 2003; Thomson *et al.*, 2005; Tao and Jiang, 2006). However, the influence of biomechanical properties and geometry of the vocal folds on phonation has not been systematically investigated. Such investigation would require a scan of the dynamic behavior of the coupled fluid-structure system over a large range of the parameter space, which is generally computationally expensive when continuum models are used. Such an approach was used in Titze and Talkin (1979) but at the cost of a reduced spatial resolution. Using a linear stability analysis approach, the influence of geometric and biomechanical properties of the vocal fold on phonation onset can be investigated at a less demanding computational cost, as shown in a recent study (Zhang *et al.*, 2007). In that paper, mechanisms of phonation onset were investigated in an isotropic two-dimensional continuum vocal fold model. They showed that the primary mechanism of phonation onset is due to the mode-coupling effect of the flow-induced stiffness, which causes two vocal fold eigenmodes to synchronize to produce an unstable eigenmode: Synchronization of two eigenmodes at the same frequency allows the flow pressure induced by one eigenmode to interact with the tissue velocity of the other eigenmode. Synchronization of two eigenmodes at the same frequency but different phases establishes a flow pressure field that is at least partially in-phase with the vocal fold velocity, allowing the cross-mode interaction to establish a net energy flow from airflow into the vocal fold tissue.

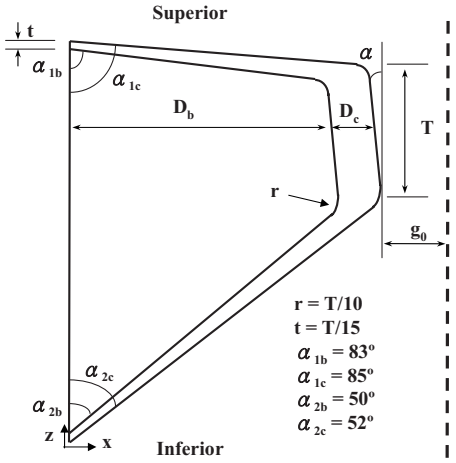

FIG. 1. The two-dimensional vocal fold model and the glottal channel. The coupled vocal fold-flow system was assumed to be symmetric about the glottal channel centerline, and only the left half of the system was considered in this study. T is the thicknesses of the medial surface of the vocal fold in the flow direction; D_b and D_c are the depths of the vocal fold body and cover layers at the center of the medial surface, respectively; g_0 is the minimum prephonatory glottal half-width of the glottal channel at rest. The divergence angle α is the angle formed by the medial surface of the vocal fold with the z-axis. Other parameters include the thickness of the cover layer at the base of the vocal fold, t, the rounding fillet radius, r, and the entrance and exit angles of the body and cover layers. The dashed line indicates the glottal channel centerline.

In this study, the influence of changes in geometry and biomechanical properties of the vocal fold on phonation onset is investigated in a continuum model of the vocal folds. The focus is to investigate the influence of the stiffness of vocal fold body and cover and vocal fold geometry on phonation threshold pressure, phonation onset frequency, vocal fold vibration, and sound production efficiency. A two-layer body-cover model of the vocal fold, as suggested by Hirano (1974), is used. The body layer consists of the muscle fibers, and the deep layer of the lamina propria. The cover layer consists of the epithelium, and the superficial and intermediate layers of the lamina propria, which have no contractile properties and are generally more pliable than the body layer (Hirano, 1974). We will show that increasing vocal fold body stiffness gradually reduces the vibration amplitude of the body layer and restricts vocal fold motion to the medial surface, which leads to increased sound production efficiency. At certain conditions, a slight change in the vocal fold stiffness or vocal fold geometry may cause phonation onset to occur at a different eigenmode, leading to a sudden change in phonation onset frequency and vocal fold vibration characteristics.

II. MODEL DESCRIPTION

Figure 1 shows a sketch of the two-dimensional continuum vocal fold model. For simplicity, a left-right symmetry in the flow field and vocal fold vibration about the glottal

channel centerline was imposed, and only half the system was considered. The vocal fold consisted of two linear plane-strain elastic layers, including a body layer and a cover layer, each with distinct Young's modulus E, Poisson's ratio ν, density ρ, and structure loss factor σ. The major geometric parameters of the vocal fold model include the thickness of the medial surface T, the depths of the body (D_b) and cover (D_c) layers at the center of the medial surface, the divergence angle of the medial surface α, and the minimum glottal half-width at rest g_0. The vocal folds were coupled to a one-dimensional potential flow driven by a given constant flow rate Q at the glottal entrance. The flow was assumed to separate from the glottal walls at a location downstream of the minimum glottal constriction whose width was 1.2 times the minimum glottal width (Lous *et al.*, 1998). A zero pressure recovery was assumed downstream of the flow separation point. As no vocal tract was considered, the flow pressure at the flow separation point was set to zero. Note that the flow separation model of this study gives only a rough estimation of the actual flow separation location (Decker and Thomson, 2007). The sensitivity of phonation onset to variations of the flow separation location was investigated in a separate study (Zhang, 2008).

A nondimensional formulation of system equations was used. The vocal fold thickness $\bar{T}$, the cover layer density $\bar{\rho}_c$, and the wave velocity of the vocal fold cover layer $\sqrt{\bar{E}_c/\bar{\rho}_c}$ were used for the reference scales of length, density, and velocity, respectively. The nondimensional variables are defined as follows:

$$
\begin{aligned}
&T = 1, \quad E_c = 1, \quad \rho_c = 1, \\
&D_b = \bar{D}_b/\bar{T}, \quad D_c = \bar{D}_c/\bar{T}, \quad g_0 = \bar{g}_0/\bar{T}, \\
&E_b = \bar{E}_b/\bar{E}_c, \quad \rho_b = \bar{\rho}_b/\bar{\rho}_c, \quad \rho_f = \bar{\rho}_f/\bar{\rho}_c, \\
&P_s = \bar{P}_s/\bar{E}_c, \quad U_j = \bar{U}_j/\sqrt{\bar{E}_c/\bar{\rho}_c}, \quad f = \bar{f}/(\sqrt{\bar{E}_c/\bar{\rho}_c}/\bar{T}),
\end{aligned}
\tag{1}
$$

where ρ_f is the density of air, U_j is the mean jet velocity, P_s is the mean subglottal pressure, and f is the phonation frequency. The subcripts b and c denote the properties of the body and cover layers, respectively. Symbols without overbars denote nondimensional variables. The physical values can be recovered by multiplying the nondimensional values by the corresponding reference scales. Note that the nondimensional body stiffness corresponds to the body-cover stiffness ratio in a dimensional format. Therefore, although the results below are discussed as a function of the nondimensional body stiffness, they could also be interpreted as a function of the body-cover stiffness ratio.

For a given flow rate Q at the glottal inlet, the analysis includes two steps. In the first step, a steady-state problem of the coupled fluid-structure system is solved to obtain the deformed vocal fold geometry and the mean flow pressure distribution along the glottal channel. In the second step, a linear stability analysis as in Zhang *et al.* (2007) is performed on the deformed state of the coupled system, and the eigenvalues and the eigenvectors of the coupled system are calculated. To differentiate from the natural modes of the vocal fold structure, these eigenmodes are referred to as fluid–structure interaction (FSI) eigenmodes. The deformed state is linearly stable if all FSI eigenvalues of the coupled system have negative growth rates. Otherwise the coupled system is linearly unstable for the given flow rate. This two-step procedure is repeated for a range of subglottal flow rates, and the phonation threshold pressure would then be the corresponding subglottal pressure at which the growth rate of one FSI eigenvalue first becomes positive.

The steady-state problem of the coupled system was solved as follows. For a given subglottal flow rate Q and a zero pressure at the point of flow separation, the mean flow pressure $P(z)$ along the vocal fold surface at locations upstream of the flow separation point was given by

$$
P(z) = \frac{1}{2}\rho_f \frac{Q^2}{H_j^2}\left(1 - \frac{H_j^2}{H^2}\right), \tag{2}
$$

where H is the glottal width along the flow direction and H_j is the glottal width at the point of flow separation. The flow pressure downstream of the flow separation point was set to zero. Note that, as mentioned above, H_j is a function of the minimum glottal half-width g and the vocal fold geometry, which are again functions of the flow pressure distribution and therefore H_j. An iterative approach was used to solve the steady-state problem. The flow pressure distribution was calculated for an initial value of H_j. The structural response under this flow pressure was then solved using the commercial finite-element-modeling package COMSOL. This deformed vocal fold surface geometry was then used to update H_j. This procedure was repeated until a satisfactory convergence in the vocal fold deformation, the flow separation point, and the minimum glottal width was reached.

The procedure of the linear stability analysis was described in detail in Zhang *et al.* (2007) and is only briefly summarized here. Readers are referred to the original paper for a detailed derivation of system equations. Governing equations for vocal fold dynamics were derived from Lagrange's equations:

$$
(M - Q_2)\ddot{q} + (C - Q_1)\dot{q} + (K - Q_0)q = 0, \tag{3}
$$

where q is the generalized coordinate vector. The three matrices M, C, and K represent the mass, damping, and stiffness matrices of the vocal fold structure, respectively. A proportional structural damping was assumed for the vocal fold material so that the structural mass and damping matrices were related by $C = \sigma\omega M$, where σ is the constant structural loss factor and ω is the angular frequency. The term $Q_2\ddot{q} + Q_1\dot{q} + Q_0 q$ in Eq. (3) is the generalized force associated with the fluctuating flow pressure along the vocal fold surface as induced by vocal fold vibration. The fluctuating flow pressure was obtained as follows. First, Bernoulli's equation and continuity equation of airflow were linearized (Zhang *et al.*, 2007) around the mean deformed state of the coupled airflow–vocal fold system, which was obtained from solving the corresponding steady-state problem. The boundary conditions for the linearized flow equations included a zero fluctuating flow velocity at the glottal entrance and a zero fluctuating pressure at the flow separation location. The

fluctuating pressure was then calculated by solving the linearized flow equations under these boundary conditions. The fluctuating flow pressure consists of three components, including a flow-induced stiffness term (proportional to vocal fold displacement and represented by matrix Q_0), a flow-induced damping term (proportional to vocal fold velocity and represented by matrix Q_1), and a flow-induced mass term (proportional to vocal fold acceleration and represented by matrix Q_2). All three matrices are functions of the jet velocity U_j, which was calculated in the steady-state problem using the imposed subglottal flow rate and the deformed vocal fold geometry. Assuming $q_0=q_0e^{st}$, Eq. (3) was solved for the FSI eigenvalues s and FSI eigenvectors q_0 for a given flow rate Q.

In Zhang *et al.* (2007), Eq. (3) was solved using the Ritz method, in which polynomial functions were used as basis functions to approximate the vocal fold displacement field. In the present study, the natural eigenmodes of the vocal fold structure were used as basis functions. The vocal fold displacement field $w=[w_x,w_z]$ was approximated as

$$w_x \approx \sum_{k=1}^{N} q_k W_{x,k}, \quad w_z \approx \sum_{k=1}^{N} q_k W_{z,k}, \tag{4}$$

where $[W_{x,k},W_{z,k}]$ was the displacement field associated with the kth natural eigenmode of the vocal fold structure, q_k is the kth generalized coordinate, and N is the number of natural modes used in the approximation. In this study, $N=10$ was used. As these natural modes contain information of the vocal fold dynamics, generally only a few natural modes are necessary to obtain solutions of reasonable accuracy, which greatly reduces computational costs. The use of natural modes as basis functions also allows vocal folds of arbitrary geometry to be analyzed with no appreciable increase in computation time. In this study, the natural modes were normalized so that the total kinetic energy of the vocal fold structure was equal to 1. The generalized force matrices (Q_0,Q_1,Q_2) were numerically evaluated using the normalized basis functions.

Note that a positive minimum glottal half-width was assumed, and only the behavior of the system around the phonation onset was investigated in this study. Vocal fold collision and its influence on phonation onset were therefore not considered.

III. RESULTS

This section is organized as follows. In Sec. III A, the influence of the body-cover stiffness ratio on phonation onset is first discussed for a straight glottal channel. The influence on phonation threshold pressure, phonation onset frequency, vocal fold vibration, and sound production efficiency is discussed. Results for convergent and divergent glottal channels are discussed in Sec. III B. Competition of coexisting instabilities for dominance at phonation onset was observed for convergent glottal channels. This is discussed in Sec. III C. Due to this competition between coexisting instabilities, a slight change in either the vocal fold stiffness or the glottal divergence angle may lead to a sudden change in phonation onset frequency, vocal fold vibration, and sound production efficiency. The influence of other model parameters is then briefly discussed in Sec. III D. Finally, the implications of the results of this study on pitch control are discussed in Sec. III E.

For the results presented below, unless otherwise stated (e.g., in Sec. III D), the following values of the model parameters were used:

$$D_b=2, \quad D_c=0.333, \quad g_0=0.03, \quad \rho_b=1, \quad \rho_f=0.001\ 17, \quad \sigma=0.4. \tag{5}$$

For a medial-surface thickness of 3 mm, Eq. (5) gives a vocal fold body depth of 6 mm, a cover depth of 1 mm, and a 0.09 mm minimum glottal half-width at rest, which roughly correspond to the nominal vocal fold geometry in Titze and Talkin (1979).

A. Influence of body-cover stiffness ratio: General trends

There have been little data available on the body-cover stiffness ratio during phonation in the literature. Although the stiffness of the nonactivated body layer may be comparable to that of the cover layer, the body-cover stiffness ratio may vary in a wide range under different activities of the TA and CT muscles (Hirano, 1974). The body-cover stiffness ratio is also expected to vary in an even larger range in pathological phonation. A large range of body-cover stiffness ratio has been used in previous modeling studies. For example, in Berry *et al.* (1994), the body-cover stiffness ratio was varied from 2 to about 13. In Titze and Talkin (1979) a ratio of 10:4:2 was used for the passive stiffnesses of the muscle, ligament, and mucosa. In the three-mass body-cover model of Story and Titze (1995), the stiffness ratio of the body and cover masses was varied in the approximate range of 4–200. In this study, similar to Titze and Talkin (1979) and Story and Titze (1995), the body-cover stiffness ratio (or body stiffness E_b) was varied in a wide range (from 1 to 100) to encompass the possible physiological range that may occur in normal and pathological phonation. In normal phonation, an increasing body-cover stiffness ratio may be realized by increased contraction of the TA muscle or reduced CT muscle contraction or a combination of both.

Figure 2 shows the phonation threshold pressure, P_{th}, the phonation onset frequency, F_0, and the prephonatory minimum glottal half-width, g, as functions of the body stiffness E_b. For a straight glottal channel $\alpha=0$ (circles in Fig. 2), both the phonation threshold pressure and the phonation onset frequency increased with increasing body stiffness E_b. This is consistent with the predictions in Zhang *et al.* (2007), which stated that both the phonation threshold pressure and the phonation onset frequency increase with the natural frequency of the vocal fold structure. In this case, the increase in the natural frequency of the vocal fold structure was caused by an increase in the body stiffness. This also explains why both P_{th} and F_0 gradually approached a plateau at large values of body stiffness. For large values of body stiffness, the natural frequencies of the two-layer vocal fold structure were primarily determined by the cover stiffness

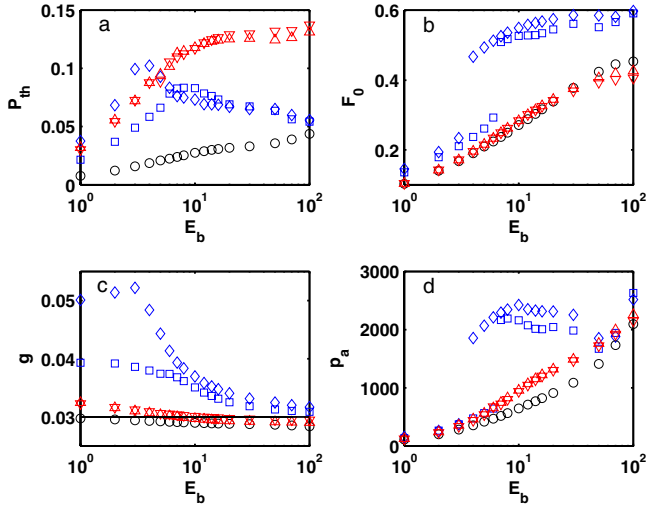

FIG. 2. (Color online) (a) Phonation threshold pressure P_{th}, (b) phonation onset frequency F_0, (c) prephonatory minimum glottal half-width g, and (d) amplitude of radiated acoustic pressure p_a as functions of body-cover stiffness ratio E_b/E_c for five different glottal channel divergence angles: ◇: −10, □: −5, ○: 0, ▽: 5, and △: 10. Also shown in (c) is the minimum glottal half-width at rest (solid line). Model parameters are given in Eq. (5).

and only increased slightly with the body stiffness. Figure 2(c) shows that the prephonatory minimum glottal half-width decreased with increasing body stiffness. A comparison between the initial and deformed vocal fold geometries shows that at small body stiffnesses, the vocal fold not only moved upwards (superiorly) but also bulged out slightly toward the glottal midline to close the glottis. As the body stiffened, the upward movement was gradually restricted and the vocal fold was forced to move more medially, leading to an even smaller prephonatory minimum glottal opening. This bulging effect was highly dependent on the vocal fold geometry (Sec. III B) and was consistently small in this case for a straight glottal channel.

The vocal fold vibration pattern at onset was calculated by substituting the corresponding eigenvector of Eq. (3) to Eq. (4). When properly scaled, the vocal fold vibration field was superimposed onto the deformed vocal fold geometry, and the corresponding vocal fold motion during one cycle can be visualized. Figures 3 and 4 show such vocal fold motion during one oscillation cycle for $E_b=1$ and $E_b=100$, respectively. The case of $E_b=1$ roughly corresponds to the first and fourth cases investigated by Story and Titze (1995), which Hirano (1974) claimed to occur when either the TA muscle is not active and the CT muscle contracts powerfully, or both the TA and CT contractions are weak. The case of $E_b=100$ roughly corresponds to the second Hirano condition and the second case in Story and Titze (1995), which may occur when the TA muscle contracts much more powerfully than the CT muscle (Hirano, 1974). Comparing Figs. 3 and 4 shows that a major difference between these two cases is that for $E_b=1$, both the body and the cover were equally involved in the vibration, whereas the body barely moved for the case of $E_b=100$. This is consistent with the description of Hirano (1974) and the observations in Story and Titze (1995) that the body layer was gradually less involved in vibration with increasing body-cover stiffness ratio. For a stiff body (Fig.

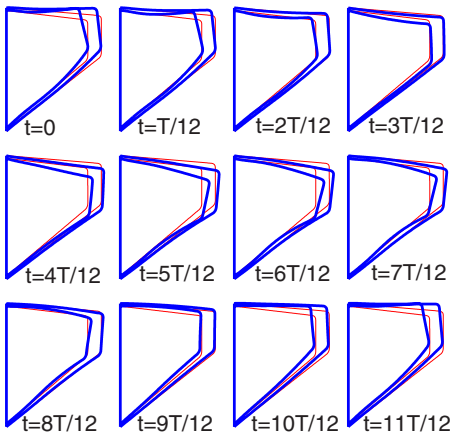

FIG. 3. (Color online) The vocal fold geometry during one oscillation cycle. $E_b/E_c=1$, $\alpha=0$ and other model parameters are given in Eq. (5). The first frame in time is shown in the leftmost plot in the first row, and the last frame is shown in the rightmost plot in the last row. The thin lines correspond to the mean deformed vocal fold geometry at onset as obtained from solving the steady-state problem.

4), the motion was restricted to the medial surface of the cover layer. The wavelength of the vibration along the medial surface was also much smaller in Fig. 4 than in Fig. 3, leading to a more wavelike motion in the case of $E_b=100$.

Figure 5 shows the vocal fold motion along the vocal fold surface as a function of superior-inferior location and time. With increasing body stiffness, regions of large-amplitude motion in both the medial-lateral and superior-inferior components were gradually reduced to the superior portion of the medial surface. In the case of $E_b=1$, the entire medial surface (spans from $z=1.8$ to 2.8 approximately) almost vibrated at the same phase. This is similar to the first and fourth cases of Story and Titze (1995) in which the upper and lower masses moved approximately in-phase. In Fig. 5(a), there is another region of in-phase motion along the inferior surface. However, the vibration amplitude in the medial-lateral direction was much weaker compared to the in-phase region along the medial surface. For the case of

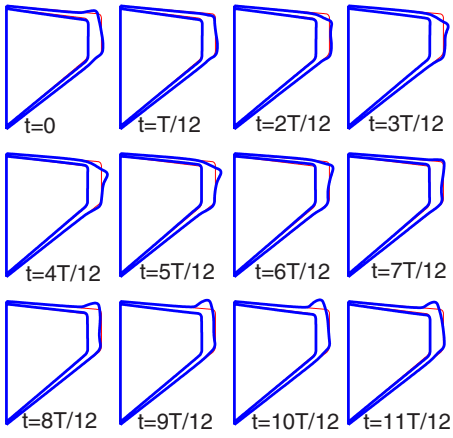

FIG. 4. (Color online) The vocal fold geometry during one oscillation cycle. $E_b/E_c=100$, $\alpha=0$, and other model parameters are given in Eq. (5). The first frame in time is shown in the leftmost plot in the first row, and the last frame is shown in the rightmost plot in the last row. The thin lines correspond to the mean deformed vocal fold geometry at onset as obtained from solving the steady-state problem.

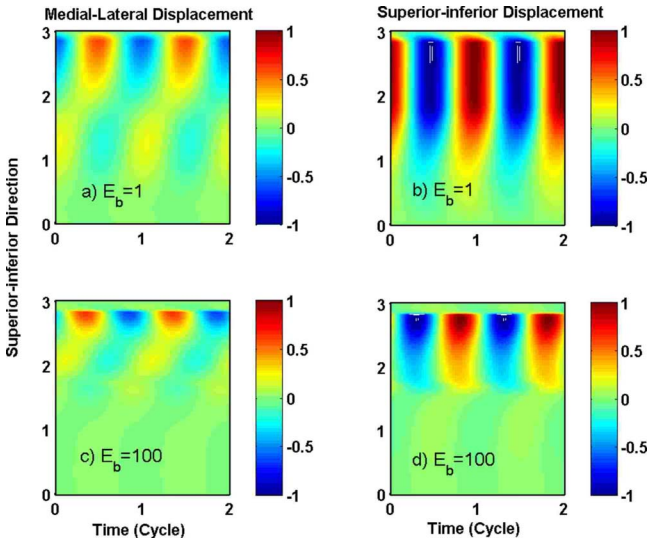

FIG. 5. (Color online) The spatiotemporal plot of the medial-lateral (left) and superior-inferior (right) components of the vocal fold surface displacement for $E_b/E_c=1$ (top) and $E_b/E_c=100$ (bottom). $\alpha=0$ and other model parameters are given in Eq. (5). For each case, the two components were normalized by the maximum value of the two components along the surface.

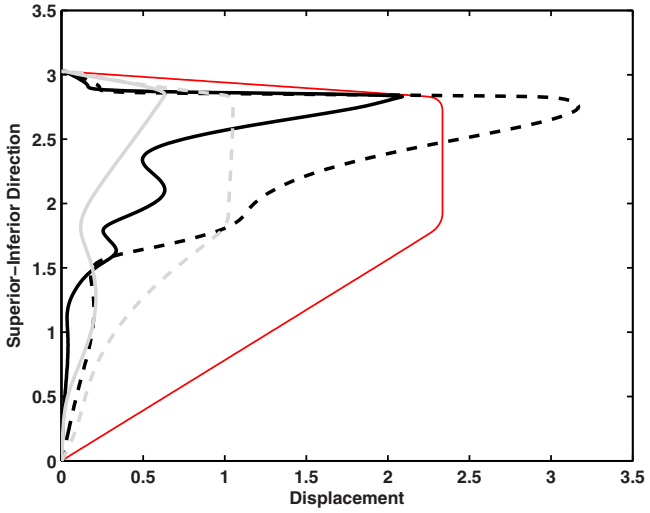

FIG. 6. (Color online) The amplitudes of the medial-lateral (thick solid lines) and superior-inferior components (dashed lines) of the vocal fold surface displacement along the flow direction for $E_b/E_c=1$ (gray lines) and $E_b/E_c=100$ (dark lines). $\alpha=0$ and other model parameters are given in Eq. (5). For each case, the FSI eigenmode was normalized so that the vibrational energy was 1. The thin solid line denotes the vocal fold surface.

$E_b=100$, the in-phase region along the medial surface was reduced in size and restricted to the superior part of the medial surface, whereas no in-phase region was observed along the inferior surface. Consequently, a phase difference can be clearly observed between the superior and inferior portions of the medial surface, with the inferior portion of the medial surface vibrating at a much smaller amplitude. This feature was not observed in any case studied by Story and Titze (1995), in which the amplitude of the lower cover mass was at least comparable to that of the upper cover mass.

Note that in both cases of Fig. 5, the vocal fold exhibited considerable superior-inferior motion. Although it was often neglected in lumped-mass models, this vertical motion was also observed in other continuum model simulations (e.g., Titze and Talkin, 1979; Berry *et al.*, 1994) and experiments (Dollinger *et al.*, 2005; Zhang *et al.*, 2006a).

The gradual confinement of large-amplitude motion to the medial surface may allow a better flow modulation and may therefore benefit sound production. Figure 6 shows the amplitudes of the medial-lateral and superior-inferior components of the vocal fold surface displacement associated with the normalized FSI eigenmode at onset for the two cases $E_b=1$ (gray lines) and $E_b=100$ (dark thick lines). For comparison between cases of different body stiffnesses, the FSI eigenvector of the coupled system for each case was normalized so that the average kinetic energy of the entire vocal fold structure over one cycle was 1. Consistent with Figs. 4 and 5, the vocal fold vibration amplitude was significantly reduced along the inferior and superior surfaces in the case of $E_b=100$ as compared to the case of $E_b=1$. For the same vibrational energy of the vocal fold structure (due to eigenvector normalization), the restriction of the vibration energy to the cover layer and the medial surface led to a much larger vibration amplitude at the superior portion of the medial surface in the case of $E_b=100$ than in the case of $E_b=1$. Note that vocal fold motion in this region (the superior portion of the medial surface) is the most effective in terms of flow modulation and affecting the intraglottal pressure distribution and is therefore the most efficient in terms of sound production.

To quantify the effect of different vocal fold vibration patterns on voice production, a sound production efficiency was defined as the amplitude of the acoustic pressure p_a radiated into an infinitely long uniform vocal tract due to vocal fold vibration associated with the corresponding *normalized* FSI eigenvector. The acoustic pressure p_a was calculated as (Zhang *et al.*, 2002)

$$p_a = -\frac{1}{2H_{\text{in}}}\int_S p n_z \cdot dS - \frac{1}{2H_{\text{in}}}\int_S \rho_f c\dot{w} \cdot n dS, \tag{6}$$

where p is the fluctuating flow pressure along the vocal fold surface S induced by the vocal fold motion w, c is the speed of sound, and n_z is the vertical component (in the flow direction) of the normal vector of the vocal fold surface pointing into the vocal fold. Note that Eq. (6) was obtained by assuming that the dimensions of the vocal folds were much smaller than the acoustic wavelength of interest so that there was no time delay between contributions to the far field sound from vocal fold motion at different spatial locations along the vocal fold surface. The terms in the right hand side of Eq. (6) include contributions of both the dipole source (due to the fluctuating transglottal pressure) and the monopole source (due to instantaneous volume change of the vocal folds) (Zhang *et al.*, 2002). The flow pressure p was calculated using the normalized FSI eigenvector of the coupled system, as described in Zhang *et al.* (2007). The acoustic pressure p_a thus calculated represented the acoustic pressure produced by vocal fold vibration of unit kinetic energy and thus quantified the voice production efficiency of the corresponding vocal fold vibration pattern. The amplitude of the calculated p_a was shown as a function of the body stiffness in Fig. 2(d). As expected, the sound production efficiency increased with

increasing body stiffness, as the vocal fold motion was gradually restricted to the cover layer and the medial surface. For all cases of this study, the contribution of the monopole source to the total acoustic pressure was negligible compared to that of the dipole source.

Although no results were shown for other values of E_b, as the body stiffness increased, the vocal fold vibration pattern evolved continuously from a vibration pattern similar to that in the case of $E_b=1$ toward one similar to the case of $E_b=100$. With increasing body stiffness, the vocal fold motion was gradually restricted to the cover layer, leading to increased sound production efficiency. As the region of in-phase large-amplitude motion was gradually reduced in size and moved to the superior portion of the medial surface, the phase difference between the superior and inferior potions of the medial surface increased with increasing body stiffness, gradually leading to a wavelike motion along the vocal fold surface.

B. Effects of glottal channel geometry

Figure 2 also shows the results obtained for nonstraight glottal channel geometries. Other model parameters were the same as given in Eq. (5). For divergent glottal channels (triangle symbols in Fig. 2) and convergent glottal channels with small body stiffnesses (diamond and square symbols in Fig. 2), similar observations as discussed in Sec. III A can be made on the variation in phonation threshold pressure, phonation onset frequency, and radiated acoustic pressure with body stiffness. In general, the phonation threshold pressures for both divergent and convergent channels were higher than those for the straight glottal channel. This difference could be due to different intraglottal pressure distributions associated with different glottal channels. Another possible explanation is that for a given minimum glottal width, the average glottal width was larger for divergent and convergent channels than the straight glottal channel, which weakened the fluid-structure coupling strength (Sec. III D). The sound production efficiency was slightly higher for divergent glottal channels and convergent channels with small body stiffnesses than for the straight glottal channel.

At small values of the body stiffness, the divergent glottis was slightly pushed open by the glottal flow. For convergent glottal channels, the glottis-opening effect was even more pronounced at small body stiffnesses, and the prephonatory glottal opening was consistently larger than the glottal opening at rest for all values of body stiffness investigated. This is probably due to the relatively high intraglottal pressure associated with convergent glottal channels. For both geometries with increasing body stiffness, the prephonatory glottal opening gradually decreased. For divergent geometries and large enough body stiffnesses ($E_b>10$), the prephonatory glottal opening was actually smaller than the glottal opening at rest. This is consistent with the observation for the straight glottis, as discussed in Sec. III A: stiffening the body restricted the vertical motion and caused the vocal fold to bulge out more in the medial direction, therefore reducing the prephonatory minimum glottal opening. This is also consistent with clinical observations that vocal folds with increased cover stiffness (e.g., for scarred vocal folds) are often blown apart by the airflow even if the glottis was closed completely at rest. In this case, surgical medialization would not improve much the voice, and other measures are required to reduce the cover stiffness (Isshiki, 1998).

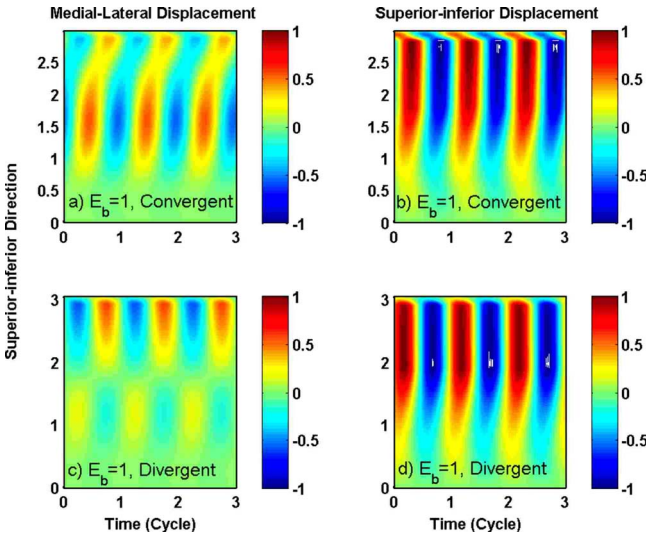

FIG. 7. (Color online) The spatiotemporal plot of the medial-lateral (left) and superior-inferior (right) components of the vocal fold surface displacement for $\alpha=-5$ (top) and $\alpha=5$ (bottom). $E_b/E_c=1$ and other model parameters are given in Eq. (5). For each case, the two components were normalized by the maximum value of the two components along the surface.

Figure 7 shows the vocal fold vibration pattern for a convergent ($\alpha=-5$) and a divergent ($\alpha=5$) glottis for $E_b=1$. The vocal fold vibration for a convergent glottis [Figs. 7(a) and 7(b)] exhibited two regions of in-phase medial-lateral vibration with comparable amplitudes, which is in contrast to only one region of dominant medial-lateral motion for a straight glottis [Fig. 5(a)]. In Fig. 7(a), one region is located in the small area around the superior edge of the medial surface, while the other spanned a much larger area in the superior-inferior direction. The vocal fold vibration within each region was almost in-phase, but the two regions vibrated slightly out-of-phase with each other. Note that the existence of two regions of in-phase motion along the medial surface is reminiscent of two lumped masses vibrating slightly out-of-phase, as described by the two-mass model of Ishizaka and Flanagan (1972).

The vocal fold vibration for a divergent glottis [Figs. 7(c) and 7(d)] was qualitatively similar to that of the straight glottis, with dominant medial-lateral vibration along the medial surface and a much weaker motion along the inferior surface. With increasing body stiffness, the region of dominant motion was gradually reduced to the superior portion of the medial surface, as in the case of a straight glottis [Figs. 5(c) and 5(d)].

C. Competition of coexisting instabilities

For convergent glottal channels with large body stiffnesses, the phonation onset pattern as a function of body stiffness was quite different from that for straight and divergent glottal channels. For small body stiffnesses, the phonation threshold pressure and the phonation onset frequency

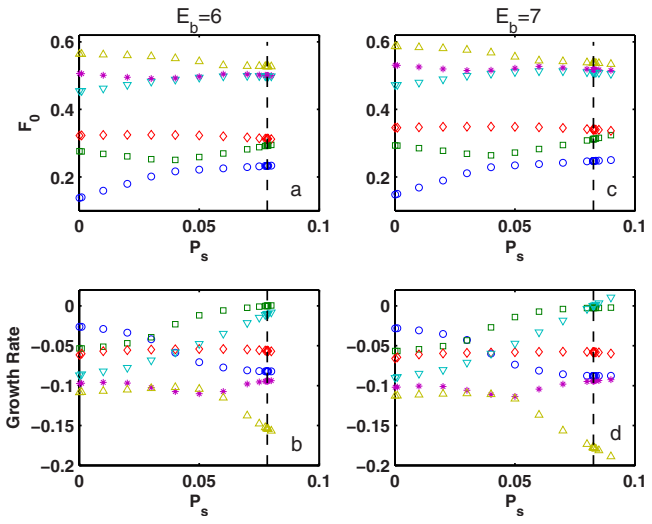

FIG. 8. (Color online) The frequencies (top) and growth rates (bottom) of the first six eigenvalues (○: first; □: second; ◇: third; ▽: fourth; ∗: fifth; △: sixth) of the coupled fluid-structure system as a function of the subglottal pressure for $E_b/E_c=6$ (left) and $E_b/E_c=7$ (right). $\alpha=-5$ and other model parameters are given in Eq. (5). The vertical line indicates the point of onset. Despite a slight change in the body-cover stiffness ratio E_b/E_c, onset occurred as a different eigenmode was destabilized.

gradually increased with increasing body stiffness, as in the cases of straight and divergent glottal channels. However, for the case of a -5 divergence angle (square symbols in Fig. 2), as body stiffness increased from 6 to 7 in Fig. 2, the phonation onset frequency abruptly increased to a much higher value, whereas the phonation threshold pressure only increased slightly. As the body stiffness further increased, the phonation onset frequency increased gradually, but the phonation threshold pressure started to decrease.

The abrupt increase in phonation onset frequency in response to a slight change in body stiffness was due to the competition of two coexisting instabilities for dominance. Figure 8 shows the frequencies and growth rates of the first six eigenvalues of the coupled system for the two cases before ($E_b=6$) and after ($E_b=7$) the abrupt increase in F_0. As shown in Fig. 8, there were two groups of eigenmodes of strong interaction: the first group included eigenmodes 1 and 2, and the second group included eigenmodes 4, 5, and possibly 6. At close to onset, there were two eigenmodes (eigenmodes 2 and 4) that had growth rate close to zero and increasing, but with quite different frequencies. For small values of body stiffness ($E_b<7$), the interaction between the first two eigenmodes was strong, and onset occurred as the second eigenmode first reached a zero growth rate. With increasing body stiffness, this interaction between eigenmodes in the first group gradually weakened [as indicated by the increasing phonation threshold pressure for $E_b<7$ in Fig. 2(a)], whereas the interaction between eigenmodes of the second group became increasingly stronger [as indicated by the decreasing phonation threshold pressure for $E_b>7$ in Fig. 2(a)]. At a certain threshold ($E_b=7$), the interaction within the second group was so strong that the fourth eigenmode reached a zero growth rate before the second eigenmode did, and phonation onset occurred at the fourth eigenmode instead of the second eigenmode, leading to an abrupt increase in phonation onset frequency.

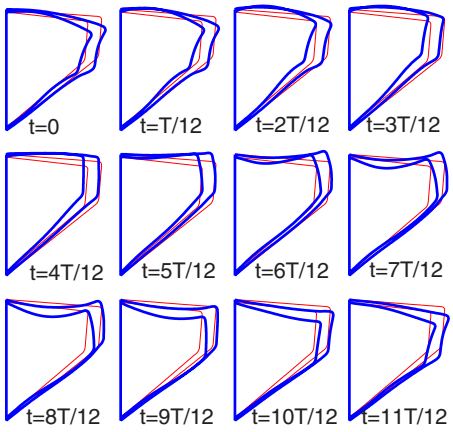

FIG. 9. (Color online) The vocal fold geometry during one oscillation cycle. $E_b/E_c=6$, $\alpha=-5$ and other model parameters are given in Eq. (5). The first frame in time is shown in the leftmost plot in the first row, and the last frame is shown in the rightmost plot in the last row. The thin lines correspond to the mean deformed vocal fold geometry at onset as obtained from solving the steady-state problem.

Figures 9 and 10 show the vocal fold motion during one oscillation cycle for the two cases $E_b=6$ and $E_b=7$, respectively. When vibrating at a higher-order eigenmode, the vocal fold vibration along the surface had a smaller wavelength in the case of $E_b=7$, as compared to the case of $E_b=6$. This led to a more wavelike motion in the case of $E_b=7$. The corresponding spatiotemporal plots are shown in Fig. 11. Compared to the case of $E_b=6$, the vocal fold vibration in the case of $E_b=7$ exhibited a large medial-lateral motion along the superior edge of the medial surface and reduced superior-inferior motion along the vocal fold surface (except the superior part of the medial surface, where the upheaval-like motion was observed in Fig. 10). Figure 12 compares the amplitudes of the medial-lateral and superior-inferior displacement of the normalized FSI eigenmode along the vocal fold surface at onset for the two cases $E_b=6$ (gray lines) and $E_b=7$ (dark thick lines). The motion was more restricted to the superior portion of the medial surface in the case of $E_b=7$. Note that the vocal fold vibration for $E_b=7$ was similar

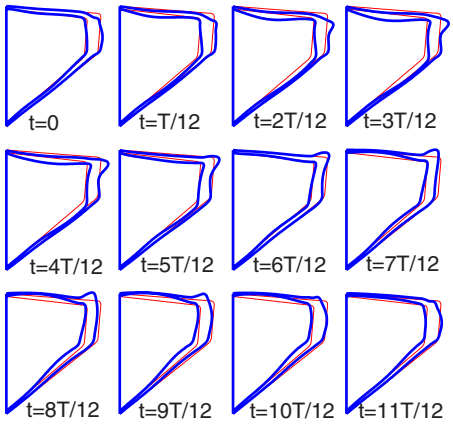

FIG. 10. (Color online) The vocal fold geometry during one oscillation cycle. $E_b/E_c=7$, $\alpha=-5$, and other model parameters are given in Eq. (5). The first frame in time is shown in the leftmost plot in the first row, and the last frame is shown in the rightmost plot in the last row. The thin lines correspond to the mean deformed vocal fold geometry at onset as obtained from solving the steady-state problem.

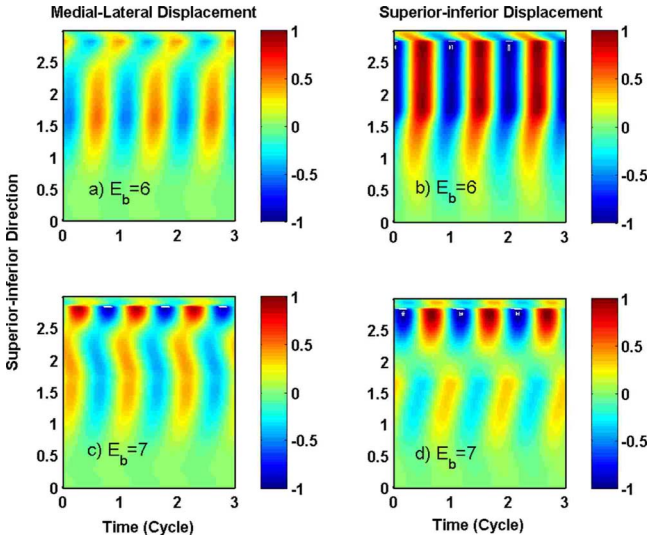

FIG. 11. (Color online) The spatiotemporal plot of the medial-lateral (left) and superior-inferior (right) components of the vocal fold surface displacement for $E_b/E_c=6$ (top) and $E_b/E_c=7$ (bottom). $\alpha=-5$ and other model parameters are given in Eq. (5). For each case, the two components were normalized by the maximum value of the two components along the surface.

to the case of $E_b=100$, in terms of the surface vibration pattern (e.g., small wavelength, wavelike motion, and restriction of large motion to the superior portion of the medial surface). However, these common features were achieved in different ways: one was induced by vibrating at a higher-order mode, while the other was induced by a stiff body.

The abrupt increase in phonation onset frequency was accompanied by a boost in sound production efficiency, as shown in Fig. 2(c). In fact, Fig. 2(c) shows that vibrating at a higher-order eigenmode was always more efficient in terms of sound production than vibrating at a lower-order mode. Although the motion was more uniformly spread over the vocal fold surface in the case of $E_b=7$, excitation of the

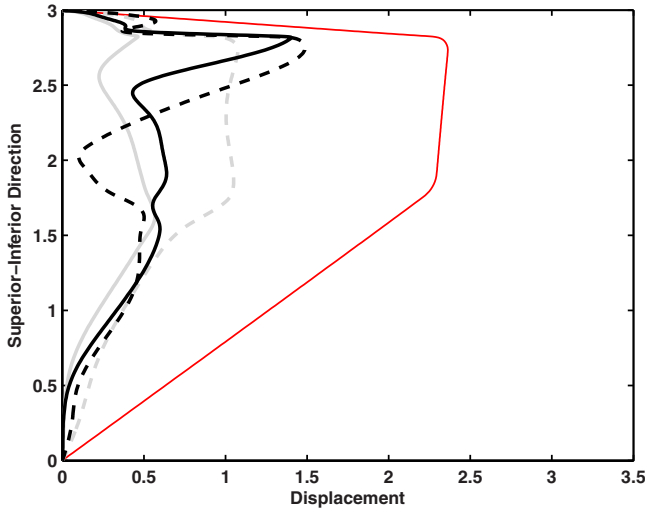

FIG. 12. (Color online) The amplitudes of the medial-lateral (thick solid lines) and superior-inferior components (dashed lines) of the vocal fold surface displacement along the flow direction for $E_b/E_c=6$ (gray lines) and $E_b/E_c=7$ (dark lines). $\alpha=-5$ and other model parameters are given in Eq. (5). For each case, the FSI eigenmode was normalized so that the vibrational energy was 1. The thin solid line denotes the vocal fold surface.

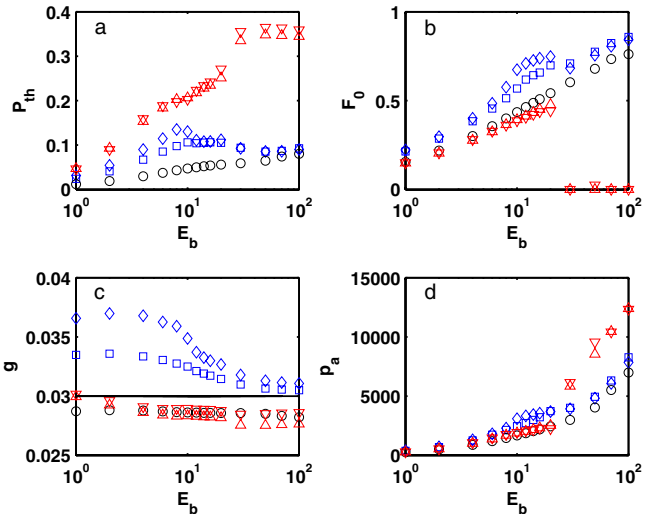

FIG. 13. (Color online) (a) Phonation threshold pressure P_{th}, (b) phonation onset frequency F_0, (c) prephonatory minimum glottal half-width g, and (d) amplitude of radiated acoustic pressure p_a as functions of body-cover stiffness ratio E_b/E_c for five different glottal channel divergence angles: ◇: −10, □: −5, ○: 0, ▽: 5, and △: 10. Also shown in (c) is the minimum glottal half-width at rest (solid line). $T=1$, $D_b=6D_c=1.2$, and other parameters are given in Eq. (5).

higher-order mode reduced the superior-inferior motion (compare $E_b=7$ in Fig. 12 to both $E_b=6$ in Fig. 12 and $E_b=100$ in Fig. 6), which allowed more energy to be spent on the medial-lateral motion at the superior portion of the medial surface and led to higher sound production efficiency.

D. Effects of other model parameters

As expected, the eigenmode synchronization pattern is highly dependent on the vocal fold geometry. As an example, Fig. 13 shows the phonation onset characteristics when the vocal fold depths were decreased [$D_b=1.2$, $D_c=0.2$, other parameters the same as in Eq. (5)], which is more similar to the conditions used in previous studies (Zhang *et al.*, 2007; Zhang, 2008). For the straight glottal channel, onset occurred due to the interaction of the first and second eigenmodes. For convergent glottal channels, onset occurred due to the interaction of the second and third eigenmodes for small body stiffnesses ($E_b<8$) but changed to the interaction of the first and second eigenmodes for large body stiffnesses ($E_b>20$). However, as the second eigenmode was involved in all cases, no abrupt change in phonation onset frequency was observed in Fig. 13. For divergent glottal channels, the synchronization pattern changed from interaction (coupled-mode flutter) between the first and second eigenmodes for small body stiffnesses ($E_b<20$) to static divergence (zero-frequency instability) at larger body stiffnesses ($E_b>20$), which is consistent with Zhang (2008). Note that for this geometry, the prephonatory minimum glottal half-width was consistently smaller than that in Fig. 2, indicating an increasing difficulty for the vocal fold to be deformed laterally with decreasing vocal fold depth (or aspect ratio).

Figures 14(a) and 14(b) show the phonation threshold pressure and phonation onset frequency as a function of the structural loss factor for $E_b=10$ and other parameter values in Eq. (5). Figures 14(c) and 14(d) show the phonation

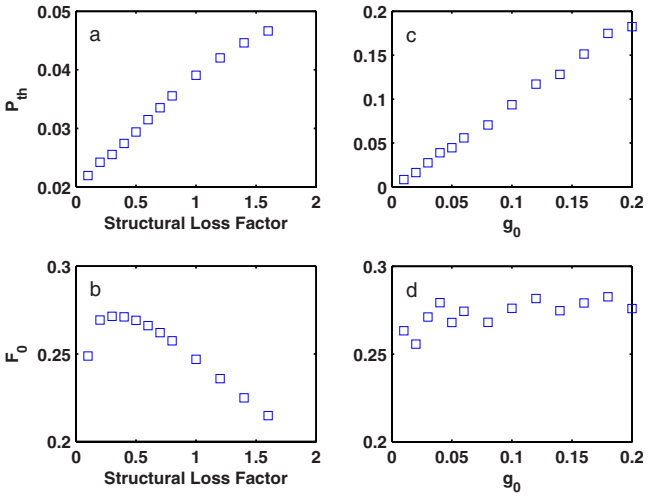

FIG. 14. (Color online) The left column shows the (a) phonation threshold pressure and (b) phonation onset frequency as functions of structural loss factor (E_b=10, g_0=0.03). The right column shows the (c) phonation threshold pressure and (d) phonation onset frequency as functions of minimum glottal half-width at rest (E_b=10, σ=0.4).

threshold pressure and phonation onset frequency as a function of the minimum glottal half-width at rest for E_b=10 and other parameter values in Eq. (5). Figure 14 shows an approximately linear dependence of the phonation threshold pressure on both the structural loss factor and the glottal half-width at rest. Although the values of model parameters do not exactly match, this almost-linear dependence is consistent with previous experimental observations (Titze *et al.*, 1995; Chan *et al.*, 1997). As there was no sudden change in the eigenmode synchronization pattern, the phonation frequency changed continuously in the case of Fig. 14. It decreased with increasing structural loss factor and slightly increased with increasing glottal half-width.

E. Implications on pitch control

The implications of the results of this study on pitch control are better illustrated using dimensional variables. Figure 15(a) shows four phonation onset frequency contours in the $\bar{E}_c - \bar{E}_b$ space corresponding to 100, 150, 200, and 250 Hz, respectively. The figure was generated from Fig. 2(b) for a straight glottal channel, a medial surface thickness T=3 mm, and a vocal fold density of 1000 kg/m^3. Figure 15 shows that the effectiveness of varying body and cover stiffness as a pitch control mechanism depends on the body-cover stiffness ratio. For very large body-cover stiffness ratios, which correspond to a case with maximum TA contraction and minimum CT contraction, phonation frequency can be effectively controlled by varying the cover stiffness, whereas varying the body stiffness as a pitch control was much less effective. For very small body-cover stiffness ratios, which correspond to a case when both the TA and CT contractions are weak or when the TA muscle is not active and the CT muscle contracts powerfully, phonation frequency can be effectively controlled by varying the body stiffness, whereas varying cover stiffness had little influence

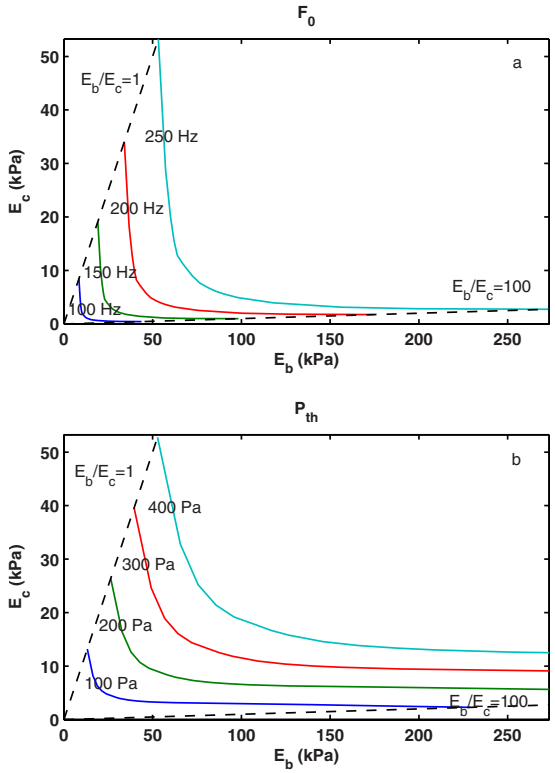

FIG. 15. (Color online) (a) Constant F_0 contours and (b) constant P_{th} contours in the $E_c - E_b$ space. T=3 mm and ρ_c=1000 kg/m^3. In (a), the four solid lines indicate F_0 of 100, 150, 200, and 250 Hz. In (b), the four solid lines indicate P_{th} of 100, 200, 300, and 400 Pa. The two dashed lines indicate constant body-cover stiffness ratio of E_b/E_c=1 and E_b/E_c=100. F_0 can be effectively controlled by changing the body stiffness at small body-cover stiffness ratios (E_b/E_c<10) and by changing the cover stiffness for large body-cover stiffness ratios (E_b/E_c>10).

on phonation frequency. For medium values of body-cover stiffness ratio, phonation frequency can be controlled by varying either the body or cover stiffness.

Figure 15(a) also shows that the same phonation onset frequency can be achieved by different combinations of body and cover stiffnesses. For example, an F_0 of 100 Hz can be achieved by $[\bar{E}_b, \bar{E}_c]$=[8.52, 8.52] kPa for E_b/E_c=1, $[\bar{E}_b, \bar{E}_c]$=[10.24, 2.05] kPa for E_b/E_c=5, or $[\bar{E}_b, \bar{E}_c]$=[43.7, 0.44] kPa for E_b/E_c=100. To produce the same F_0 of 100 Hz, the condition of E_b/E_c=5 required moderate values of both the body and cover stiffnesses. For body-cover stiffness ratios below or above 5, producing the same F_0 required a dramatic increase in either the cover stiffness (increased from 2.05 to 8.52 kPa) or the body stiffness (from 10.24 to 43.7 kPa). In human phonation, this dramatic increase would require strong contraction of either the CT or TA muscles in human phonation, which may be less desirable.

Figure 15(b) shows similar contour plots for phonation threshold pressure. As the phonation threshold pressure is directly related to the phonation onset frequency, a similar behavior can be also noted as to the effectiveness of varying body or cover stiffness as a control mechanism of phonation threshold pressure.

Note that in reality, the variations in body and cover stiffnesses are often accompanied by changes in the vocal

fold geometry. This effect needs to be taken into consideration using a proper muscular model (e.g., Titze and Hunter, 2007) in order to obtain a complete understanding of pitch control mechanisms in human phonation.

IV. DISCUSSION

The mucosal wave along the vocal fold surface has long been observed and considered an essential element of vocal fold vibration. It is generally assumed that mucosal wave propagation causes a time delay in the movement from bottom to top of the vocal folds (Titze, 1988) or a phase difference between the upper and lower masses in the two-mass model. However, the present study and a previous study (Zhang *et al.*, 2007) show that the phase difference of the vocal fold vibration along the vocal fold surface was the consequence of eigenmode synchronization at the same frequency but different phases. A wavelike motion appears only for vibrations of small wavelengths, which occurred in this study at large body-cover stiffness ratios (Sec. III A) or when the vocal fold vibrated at a higher-order mode (Sec. III C). In general, the vocal fold vibration does not necessarily exhibit a wavelike motion. More often, two regions of almost-in-phase vocal fold motion were observed along the vocal fold surface, and noticeable phase change only occurred in the transition region. There was no wave propagation (or rather infinitely fast wave motion) within each in-phase region. In other words, the presence of mucosal wave is not a necessary component of the self-sustained vocal fold vibration. However, the presence of mucosal wave may be desirable in phonation, for example, to achieve high sound production efficiency, as shown in this study.

This study shows that the concept of eigenmode and eigenmode synchronization may provide a theoretic framework toward a better understanding of the correspondence between biomechanical and geometric properties of the vocal folds and the resulting phonation characteristics. In this study, the vocal fold vibration was calculated as the weighted combination of the natural modes of the vocal fold structure, with the weights (the generalized coordinates q) determined by the fluid-structure interaction or the eigenmode synchronization process. With different combinations of weights, various types of vocal fold vibration can be generated, as demonstrated in this study. Therefore, further research on phonation onset can be pursued in two aspects. The first aspect focuses on the natural modes and how they would be affected by the changes in geometric and biomechanical properties of the vocal fold structure. Such study would yield valuable information on the characteristic vocal fold vibration patterns and the associated frequencies (e.g., Titze and Strong, 1975; Berry and Titze, 1996; Cook and Mongeau, 2007). For example, the restriction of motion toward the cover layer and the superior portion of the medial surface with increasing body stiffness can be explained by similar features in the first few natural modes of the vocal fold structure as the body stiffness increases. The second aspect aims to investigate eigenmode synchronization due to the fluid-structure interaction and to determine the weights used to calculate the final vocal fold vibration (e.g., Zhang *et al.*, 2007). Such studies would reveal which modes have a strong interaction and eventually synchronize to induce phonation onset and at what conditions bifurcations [e.g., the abrupt frequency change in Fig. 2(b)] in the behavior of the coupled system would occur.

This study shows that a slight change in body stiffness can cause an abrupt change in phonation onset frequency and vocal fold vibration pattern. Although this study focuses on phonation onset, it is reasonable to expect that a similar mechanism may also be present in finite-amplitude vibrations beyond onset and may play a role in register change. This mechanism requires that the coupled system have two or more coexisting instabilities so that, given appropriate changes in certain system parameters, the vocal fold vibration can switch from one self-oscillating state to another. For example, Tokuda *et al.* (2007) showed that a qualitative change in the vocal fold vibration and phonation frequency in a three-mass model was observed when two synchronizing eigenmodes switched from the first and second eigenmodes to the second and third eigenmodes. Note that these instabilities could be two near-field FSI instabilities (instabilities due to two pairs of synchronizing eigenmodes, as in the case of Fig. 8) but could also be one near-field FSI instability and one due to the coupling of the vocal fold vibration to sub- or supraglottal acoustics (Zhang *et al.*, 2006a, 2006b).

Although such abrupt change in vocal fold vibration pattern in Tokuda *et al.* (2007) and the present study was induced by a slight change in vocal fold stiffness, a similar abrupt change may be also induced by changes in other system parameters, which may affect the relative strength of the coexisting instabilities. Such parameters include flow separation point (as induced by change in flow rate or vocal fold geometry, Zhang, 2008), coupling to the sub- or supraglottal acoustics (Zhang *et al.*, 2006a, 2006b), and vocal fold geometry (Titze, 1994). For example, the abrupt change in vocal fold vibration pattern and phonation onset frequency, as observed in Fig. 2(b), can be also induced when the medial-surface shape changes from straight to convergent, without changing the body stiffness. This can be caused by the activation of the TA muscle, which may cause the inferior portion of the medial surface to bulge out. Such change in vocal fold geometry as induced by the contraction of the TA muscle has been suggested as a possible mechanism of register transition from chest to falsetto (Titze, 1994).

V. CONCLUSIONS

Using a linear stability analysis, phonation threshold pressure, phonation onset frequency, vocal fold vibration pattern, and sound production efficiency were investigated as a function of the mechanical and geometric parameters of a body-cover vocal fold model. The conclusions are as follows:

(1) Increasing body-cover stiffness ratio gradually restricted the vocal fold motion to the cover layer and the medial surface where the vocal fold motion is the most effective in terms of flow modulation, leading to increased voice production efficiency.

(2) A wave like motion was observed for vocal fold surface vibration of small wavelengths, which occurred at high body-cover stiffness ratios or when the vocal fold vibrated at a higher-order mode.
(3) In addition to a reduced wavelength along the vocal fold surface, self-oscillations at higher-order modes exhibited reduced superior-inferior motion. This allowed more energy to be spent on the medial-lateral motion along the superior portion of the medial surface and therefore higher sound production efficiency than that when the vocal fold vibrated at low-order modes.
(4) For small body-cover stiffness ratios, phonation onset frequency can be effectively controlled by varying the body stiffness, whereas for larger body-cover stiffness ratios, phonation onset frequency can be more effectively controlled by varying the cover stiffness.
(5) There was more than one group of eigenmodes that synchronized toward phonation onset in the coupled continuum system so that at least two potential instabilities (coupled-mode flutter in this study) existed. At certain conditions, the phonation threshold pressures associated with two such instabilities may be close to each other, and a slight change in the mechanical or geometric parameters of the system would cause phonation onset to switch from one instability to another, leading to sudden changes in (a) phonation onset frequency, (b) vocal fold vibration pattern, and (c) sound production efficiency. It is hypothesized that a similar mechanism may play a role in register change.

ACKNOWLEDGMENTS

This study was supported by research Grant Nos. R01 DC009229 and R01 DC003072 from the National Institute on Deafness and Other Communication Disorders, the National Institutes of Health.

Alipour, F., Berry, D. A., and Titze, I. R. (**2000**). "A finite-element model of vocal-fold vibration," J. Acoust. Soc. Am. **108**, 3003–3012.
Berry, D. A., Herzel, H., Titze, I. R., and Krischer, K. (**1994**). "Interpretation of biomechanical simulations of normal and chaotic vocal fold oscillations with empirical eigenfunctions," J. Acoust. Soc. Am. **95**, 3595–3604.
Berry, D. A., and Titze, I. R. (**1996**). "Normal modes in a continuum model of vocal fold tissues," J. Acoust. Soc. Am. **100**, 3345–3354.
Chan, R., Titze, I. R., and Titze, M. (**1997**). "Further studies of phonation threshold pressure in a physical model of the vocal fold mucosa," J. Acoust. Soc. Am. **101**, 3722–3727.
Colton, R. H., and Casper, J. K. (**1996**). *Understanding voice problems: A physiological perspective for diagnosis and treatment* (Lippincott Williams & Wilkins, Baltimore, MD).
Cook, D., and Mongeau, L. (**2007**). "Sensitivity of a continuum vocal fold model to geometric parameters, constraints, and boundary conditions," J. Acoust. Soc. Am. **121**, 2247–2253.
De Oliveira Rosa, M., Pereira, J. C., Grellet, M., and Alwan, A. (**2003**). "A contribution to simulating a three-dimensional larynx model using the finite element method," J. Acoust. Soc. Am. **114**, 2893–2905.
Decker, G. Z., and Thomson, S. (**2007**). "Computational simulations of vocal folds vibration: Bernouli versus Navier-Stokes," J. Voice **21**, 273–284.
Dollinger, M., Tayama, N., and Berry, D. A. (**2005**). "Empirical eigenfunctions and medial surface dynamics of a human vocal fold," Methods Inf. Med. **44**, 384–391.
Hirano, M. (**1974**). "Morphological structure of the vocal cord as a vibrator and its variations," Folia Phoniatr. **26**, 89–94.
Ishizaka, K., and Flanagan, J. L. (**1972**). "Synthesis of voiced sounds from a two-mass model of the vocal cords," Bell Syst. Tech. J. **51**, 1233–1267.
Ishizaka, K., and Flanagan, J. L. (**1977**). "Acoustic properties of longitudinal displacement in vocal cord vibration," Bell Syst. Tech. J. **56**, 889–918.
Isshiki, N. (**1998**). "Mechanical and dynamic aspects of voice production as related to voice therapy and phonosurgery," J. Voice **12**, 125–137.
Lous, N. J. C., Hofmans, G. C. J., Veldhuis, R. N. J., and Hirschberg, A. (**1998**). "A symmetrical two-mass vocal-fold model coupled to vocal tract and trachea, with application to prosthesis design," Acta Acust. **84**, 1135–1150.
Story, B. H., and Titze, I. R. (**1995**). "Voice simulation with a body-cover model of the vocal folds," J. Acoust. Soc. Am. **97**, 1249–1260.
Svec, J. G., Schutte, H. K., and Miller, D. G. (**1999**). "On pitch jumps between chest and falsetto registers in voice: Data from living and excised human larynges," J. Acoust. Soc. Am. **106**, 1523–1531.
Tao, C., and Jiang, J. J. (**2006**). "Simulation of vocal fold impact pressures with a self-oscillating finite-element model," J. Acoust. Soc. Am. **119**, 3987–3994.
Thomson, S. L., Mongeau, L., and Frankel, S. H. (**2005**). "Aerodynamic transfer of energy to the vocal folds," J. Acoust. Soc. Am. **118**, 1689–1700.
Titze, I. R. (**1988**). "The physics of small-amplitude oscillation of the vocal folds," J. Acoust. Soc. Am. **83**, 1536–1552.
Titze, I. R. (**1994**). *Principles of Voice Production* (Prentice-Hall, Englewood Cliffs, NJ).
Titze, I. R., and Hunter, E. J. (**2007**). "A two-dimensional biomechanical model of vocal fold posturing," J. Acoust. Soc. Am. **121**, 2254–2260.
Titze, I. R., Jiang, J., and Drucker, D. G. (**1988**). "Preliminaries to the body-cover theory of pitch control," J. Voice **1**, 314–319.
Titze, I. R., Schmidt, S., and Titze, M. (**1995**). "Phonation threshold pressure in a physical model of the vocal fold mucosa," J. Acoust. Soc. Am. **97**, 3080–3084.
Titze, I. R., and Strong, W. J. (**1975**). "Normal modes in vocal cord tissues," J. Acoust. Soc. Am. **57**, 736–744.
Titze, I. R., and Talkin, D. T. (**1979**). "A theoretical study of the effects of various laryngeal configurations on the acoustics of phonation," J. Acoust. Soc. Am. **66**, 60–74.
Tokuda, I. T., Horacek, J., Svec, J. G., and Herzel, H. (**2007**). "Comparison of biomechanical modeling of register transitions and voice instabilities with excised larynx experiments," J. Acoust. Soc. Am. **122**, 519–531.
Zhang, Z. (**2008**). "Influence of flow separation location on phonation onset," J. Acoust. Soc. Am. **124**, 1689–1694.
Zhang, Z., Mongeau, L., and Frankel, S. H. (**2002**). "Experimental verification of the quasi-steady approximation for aerodynamic sound generation by pulsating jets in tubes," J. Acoust. Soc. Am. **112**, 1652–1663.
Zhang, Z., Neubauer, J., and Berry, D. A. (**2006a**). "Aerodynamically and acoustically driven modes of vibration in a physical model of the vocal folds," J. Acoust. Soc. Am. **120**, 2841–2849.
Zhang, Z., Neubauer, J., and Berry, D. A. (**2006b**). "The influence of subglottal acoustics in laboratory models of phonation," J. Acoust. Soc. Am. **120**, 1558–1569.
Zhang, Z., Neubauer, J., and Berry, D. A. (**2007**). "Physical mechanisms of phonation onset: A linear stability analysis of an aeroelastic continuum model of phonation," J. Acoust. Soc. Am. **122**, 2279–2295.